Materials and Design 179 (2019) 107889

Contents lists available at ScienceDirect

Materials and Design

journal homepage: www.elsevier.com/locate/matdes

Poling-free spinning process of manufacturing piezoelectric yarns for textile applications

Sarang Park [a], Youbin Kwon [a], Minchang Sung [a], Byoung-Sun Lee [a], Jihyun Bae [b], Woong-Ryeol Yu [a,*]

[a] Department of Materials Science and Engineering and Research Institute of Advanced Materials (RIAM), Seoul National University, Seoul 08826, Republic of Korea
[b] Department of Clothing & Textiles, Hanyang University, Seoul 04763, Republic of Korea

HIGHLIGHTS

- Poling-free spinning process was designed for piezoelectric nanofiber yarns.
- PVDF-TrFE nanofibers were enhanced in both crystallinity (by 83%) and β phase ratio (by 12%) after yarn spinning process.
- Piezoelectric yarn showed high mechanical (tensile strength of ~25 MPa) and piezoelectric (potential of 500 mV and g_{33} of 0.40) properties.

GRAPHICAL ABSTRACT

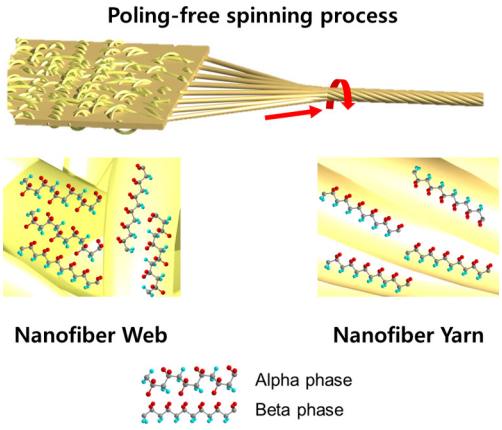

ARTICLE INFO

Article history:
Received 8 April 2019
Received in revised form 24 May 2019
Accepted 24 May 2019
Available online 28 May 2019

Keywords:
Piezoelectric yarns
Twist-spinning
PVDF nanofibers
Crystalline

ABSTRACT

This report describes a new twist-spinning process for the manufacture of piezoelectric yarn without the need for additional poling processes. Poly(vinylidene fluoride-trifluoroethylene) (PVDF-TrFE) nanofibers were first electrospun and organized into a web structure. Using rotational and translational motors, the nanofibers of the web were pulled and stretched and, finally, twisted into piezoelectric yarns. The crystallinity, β phase ratio, and mechanical and piezoelectric properties of these twist-spun piezoelectric yarns were characterized to assess the effects of the twist-spinning operation on their microstructure and performance. Twist-spun piezoelectric yarns that had undergone high degrees of stretching exhibited enhancements in both crystallinity and β phase ratio by 83% and 12%, respectively. In contrast, high stretching reduced the tensile strength and modulus of the yarns due to small surface angles. The twist-spun piezoelectric yarn with the highest β phase ratio and lowest modulus attained in this study yielded a piezoelectric potential and piezoelectric voltage constant of 500 mV and 0.412 mVm/N, respectively.

1. Introduction

Piezoelectric textiles have been suggested for use in wearable device applications due to their stable energy conversion properties, high

* Corresponding author.
E-mail address: woongryu@snu.ac.kr (W.-R. Yu).

https://doi.org/10.1016/j.matdes.2019.107889

sensitivities, and stable mechanical properties. Early research into piezoelectric textiles was carried out with a simple woven structure [1–6]. Such structures can apply compressive or tensile stresses onto piezoelectric yarns. Recently, other textile designs, including knitted [7,8] and braided [9] structures, have been used to make piezoelectric textiles. Piezoelectric textiles have been used in motion sensors on joints in fingers and arms [10,11], in systems designed to harvest energy from the human body [12–14], in motion-powered electronic skin [15], and in a self-powered breath sensor [16]. In addition, biocompatible piezoelectric textiles have been used in artificial cell scaffolds [17], cell-powered biological sensors [18], and cochlear implants [19,20]. The development of piezoelectric textiles depends on the development of piezoelectric fibers or yarn. As with most polymers, the one-dimensional nature of piezoelectric fibers allows for chain alignment and tailorable mechanical properties, affording a high degree of crystallinity and piezoelectric properties.

Fibers for piezoelectric textiles need to be both highly flexible and stretchable. Natural piezoelectric polymers such as cellulose [21] and PVDF [22] have been used to manufacture piezoelectric fibers. In general, there are two types of manufacturing method for piezoelectric fibers: melt-spinning and electrospinning. Melt spinning processes allow for low-porosity fibers with controlled diameter. However, molecular dipoles in melt-spun polymers are randomly oriented and additional poling processes [5,23,24] are required to bring them into alignment to obtain a useful piezoelectric material. Poling processes, such as contact poling or corona poling, require an ultrahigh electric field (~10 MV/m). In contrast, electrospinning does not require an additional poling process due to the high electric field applied during manufacturing [25–28]. Electrospinning processes produce fine nanofibers (or ~1 μm microfibers), which can be spun into nanofiber yarns. Piezoelectric nanofiber yarns have been manufactured using a converted electrospinning system [29] and by twisting nanofiber ribbons [30,31]. However, these yarning processes also require poling. This requirement has led to a great deal of research into new yarning processes that can yield diameter-controlled, piezoelectric yarns without poling.

This study describes the development of a twist-spinning process that can be used to produce various piezoelectric yarns from a piezoelectric nanofiber web. In literature, PVDF copolymers are poled during electrospinning process under applied electric potential. Since the poling direction is the same as the direction of the electric field [32–34], the electrospun nanofibers are used as a piezoelectric film sandwiched with two electrode films. In our study, the nanofibers were reoriented and spun into yarns, meaning that the poling became invalid in the yarn level because only the backbone chains of nanofibers maintained the poled direction (i.e., the poling effect of electrospinning process is valid only in as-spun film form). Therefore, nanofiber yarns have frequently been re-polled after electrospinning process [29–31]. There are few publications reporting the piezoelectric yarn manufactured from nanofiber webs without additional poling process. We demonstrated increased crystallinity and beta phase ratio during the yarn manufacturing process. In literature, films have been used to be stretched for high crystallinity and beta phase ratio, but there was a limit to this because of weak film properties [35]. When a nanofiber web was stretched, the nanofibers were aligned at first and were then easily torn because their inter-friction was very weak. However, the nanofibers in yarns are condensed in the radial direction under the tensile force applied and the friction force between nanofibers becomes large. Therefore, nanofiber webs can be pulled out and aligned before the failure and are then spun into yarns by the twisting process without tearing. This is the basic mechanism of poling-free piezoelectric yarn manufacturing with large stretching effect. Randomly oriented PVDF-TrFE nanofibers that had been manufactured by electrospinning were pulled from the nanofiber web, which induced molecular alignment along the pulling direction, and twisted into a yarn structure. This simultaneous alignment and stretching imparted enhanced piezoelectric properties to the resulting PVDF-TrFE nanofiber yarn without poling. We demonstrate herein that piezoelectric yarns with various microstructures and piezoelectric properties can be manufactured by controlling the spinning conditions.

2. Experimental

2.1. Yarn preform synthesis

Poly(vinylidenefluoride-trifluoroethylene) (PVDF-TrFE) copolymer (PVDF with 25 mol% of typical TrFE, Piezotech FC25, Alkema) was used to synthesize piezoelectric fibers. PVDF-TrFE was dissolved to a concentration of 21 wt% in a 3:2 (v/v) mixture of *N*,*N*-dimethylformamide (purity 99.5%; Daejung Chemical) and acetone (purity 95%; Daejung Chemical). A nanofiber web was generated as a yarn preform on aluminum foil via a single-nozzle electrospinning process under the following conditions: 22 gauge nozzle, a flow rate of 0.5 mL/h, a tip-to-collector distance of 15 cm, and an applied voltage of 15 kV.

2.2. Yarn spinning processes

The electrospun nanofiber web was spun into a nanofiber yarn using a draw-and-twist process. First, edges of the nanofiber web were fixed in a fiber grip. The fiber grip was connected to a moving motor. As the motor moved, nanofibers were pulled from the web and aligned under the resulting tension. The aligned nanofibers were then twisted into a nanofiber yarn (Fig. 1). Twist per meter (TPM) is an important parameter to describe the process parameter in the yarn manufacturing and to explain the structure of yarns. As such, TPM is defined using the process parameters in yarn spinning process such as winding speed, rotating speed, and the diameter of roller [36–42]. In our study of nanofiber yarn manufacturing, TPM was defined based on our experimental setup as follows.

$$\text{TPM (twist per meter)} = \frac{\textit{twisting speed (RPM, twist/minute)}}{\textit{translational speed (mm/ sec)}} \quad (1)$$

Since the twisting speed was fixed to 60 RPM (i.e., 1 twist/s), TPM was inversely proportional to the translational speed. The two speeds were schematically explained in Fig. 1 of the revised manuscript. As the translational speed of a spinning motor increased (i.e., TPM decreased), the nanofibers were stretched by a strong force. This is why we presented TPM from 1000 to 200 TPM in descending order, not from 200 to 1000 TPM in ascending order. During this process, a triangle was formed between the web and yarn (Fig. 2). The base of this triangle was the width of nanofiber web, and the yarn was formed in vertex point of this triangle. As the spinning motor moved in translation direction, the triangle moved to the web, and the area was fixed. Nanofibers were pulled out from the base, and the nanofiber yarn was spun in vertex with constant height of triangle.

2.3. Material characterization

The morphology of the resulting piezoelectric yarn was investigated by field-emission scanning electron microscopy (FE-SEM; SUPRA 55VP; Carl Zeiss, Germany) and yarn crystallinity was examined by X-ray diffraction (XRD; SmartLab; Rigaku, Japan), differential thermal analysis (DSC; DSC 823e; Mettler Toledo, USA), and Fourier transform infrared spectroscopy (FTIR; TENSOR27; Bruker, Germany).

The mechanical properties of nanofiber yarns were measured using a single-strand method (Fig. S1). Yarns were fixed by yarn grips featuring frictionless loops and tensile tests were performed on a universal testing machine (Quasar 5, Galdabini, Italy). The gauge length of each yarn was 20 cm and the strain rate was 8 mm/s. All of the test conditions satisfied the standards of ASTM D2256.

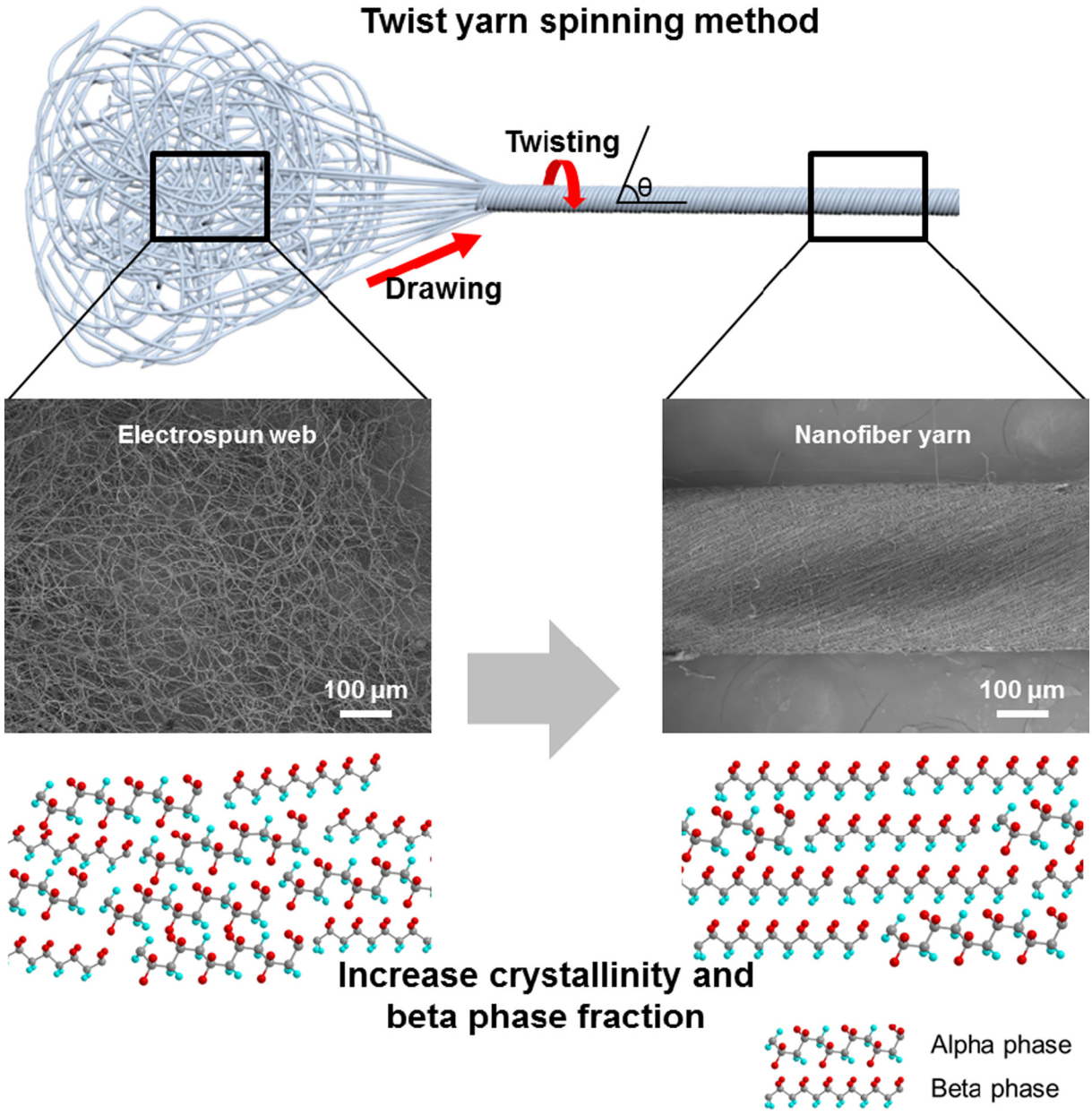

Fig. 1. Schematic diagram of the twist-spinning method and the resulting nanostructures of PVDF-TrFE nanofiber yarns.

The piezoelectric performance of the yarns was characterized using the Measurement and Analysis System of Static/Dynamic Tactile Sensors (Teraleader Inc., Korea) (Fig. S2). The PVDF-TrFE yarns were stacked into three layers separated by copper films as electrodes (Fig. S3). The stacked yarns were fixed in a 1 mm^2 area and aligned triaxially (uniaxially in each layer). A piezoelectric potential was induced under compressive stress on the yarns. The compressive stress was applied in two modes: a repeating rectangular function and an increasing rectangular function at 0.5 Hz (Fig. S4). To compare the intrinsic piezoelectric properties of the PVDF-TrFE yarns, piezoelectric voltage constants, g_{33}, were measured under the increasing stress mode.

3. Results and discussion

3.1. Morphologies of piezoelectric yarns

The morphologies of piezoelectric nanofiber yarns manufactured from an electrospun nanofiber web are shown in Fig. 2. PVDF-TrFE nanofibers were well-aligned within the yarn structures compared to those in the nanofiber web. Higher translational speeds during the twisting process yielded greater degrees of fiber stretching but also decreased the TPM of nanofiber yarns. As TPM decreased, piezoelectric yarns got thinner and exhibited smaller surface angles. A quantitative characterization of yarn morphology is shown in Fig. 3. The average diameter of the piezoelectric yarns decreased (619, 568, 494, 422, and 379 μm) with decreasing TPM (1000, 800, 600, 400, and 200), respectively. Before being twisted into a yarn, high translational speeds during pulling and alignment resulted in thin nanofiber assemblies. The nanofiber yarn was also stretched by the translational force during spinning, resulting in thinner piezoelectric yarns with low TPM. Diameter distributions of nanofibers in the preform web and piezoelectric yarns were obtained from SEM micrographs of 200 nanofibers. Fig. 3 shows that the average diameters of nanofibers in the web and yarns made with 1000, 800, 600, 400, and 200 TPM were 1261, 1126, 1046, 919, 833, and 563 nm, respectively (see Fig. S5 for SEM micrographs). These data imply that nanofibers were thinned during the spinning process

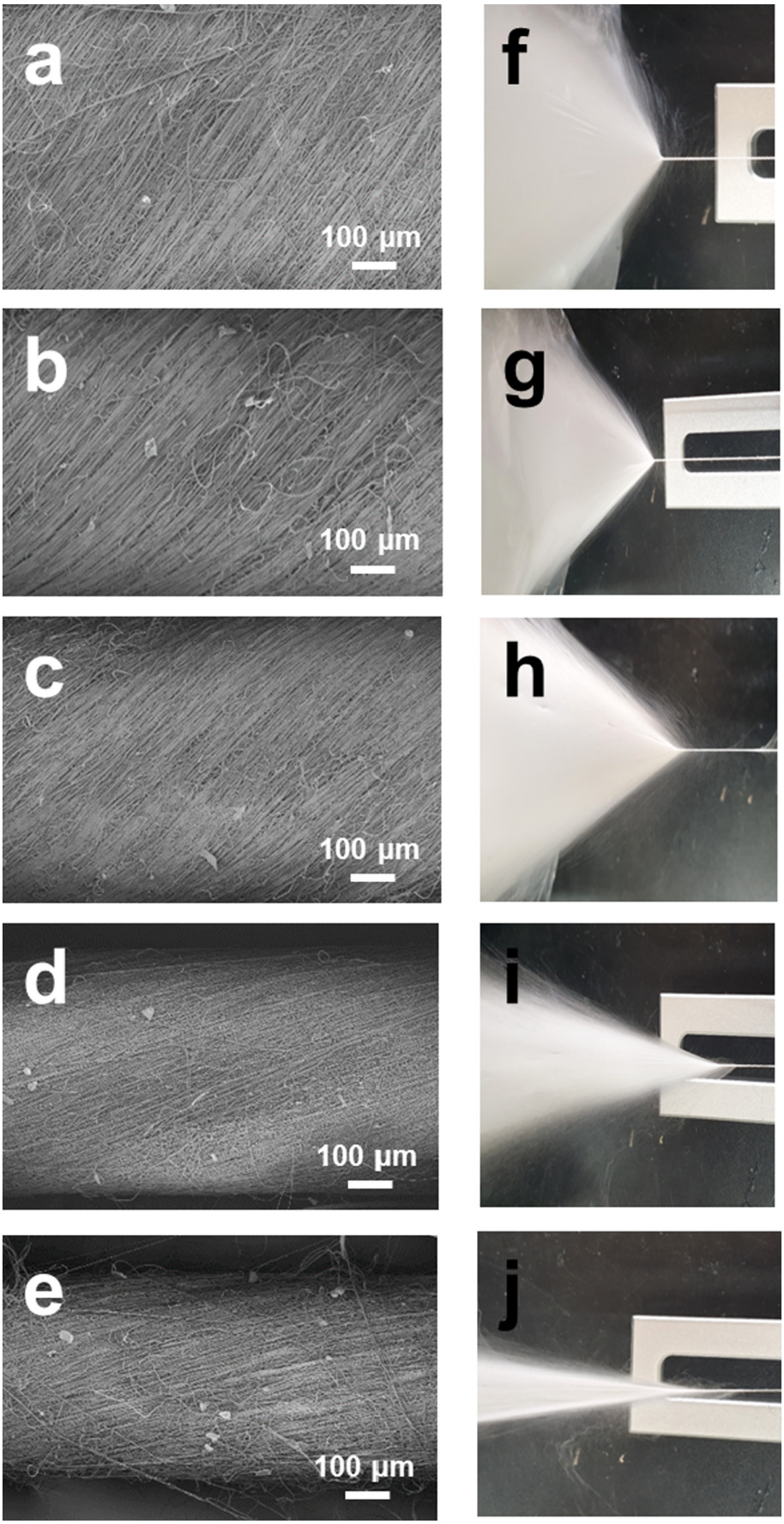

Fig. 2. SEM images of PVDF-TrFE piezoelectric nanofiber yarns and spinning photographs. (a, f) 1000 TPM (b, g) 800 TPM (c, h) 600 TPM (d, i) 400 TPM, and (e, j) 200 TPM yarn.

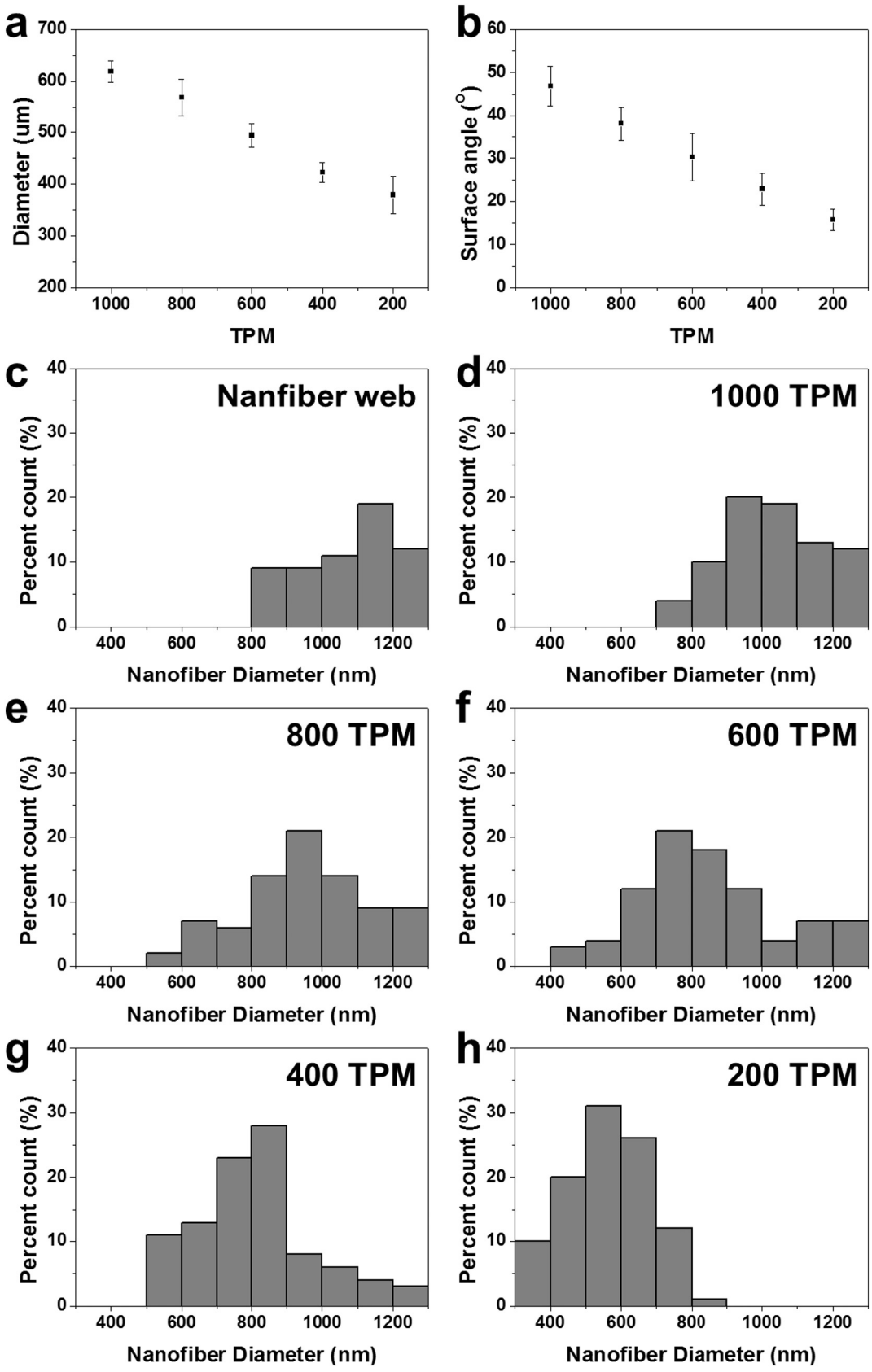

Fig. 3. The effect of TPM on the (a) diameter and (b) surface angle of PVDF-TrFE piezoelectric nanofiber yarns. The diameter distributions are shown for nanofibers in (c) the preform web and (d–h) piezoelectric yarns.

and that the thinning effect was proportional to the translational speed. This may be due to the glass transition temperature of PVDF-TrFE (ca. −28 °C), which is much lower than room temperature. During yarn spinning, nanofibers are drawn smoothly and exhibit rubbery behaviors with plastic deformation. Since the drawing of nanofibers can enhance the crystallinity of yarns, which is an important factor in determining piezoelectric properties, the thinner nanofibers are expected to show enhanced piezoelectric properties.

The surface angle of our piezoelectric yarns decreased from 46.9° to 37.9°, 30.2°, 22.8°, and 15.7° for yarns with 1000, 800, 600, 400, and 200 TPM, respectively (Figs. 4d-4h). During yarn spinning, nanofibers were pulled out and aligned prior to being twisted, forming a triangle (Fig. 2) from the web to the yarn. At the same RPM during twisting, the base of this triangle remains constant. However, the height of the triangle increases as the translational speed of the twisting motor increases and greater translational forces are applied. The triangle becomes larger and the angle opposite the base becomes smaller. Thus, the initial surface angle of our nanofiber yarns decreased with increasing translational speed of the twisting motor.

3.2. Structural characterization

The crystal structures of our piezoelectric yarns were investigated using XRD, DSC, and FTIR (Fig. 4). The peak at $2\theta = 19.8°$ in the X-ray diffractogram in Fig. 4a represents (200) reflections of the β phase with fully-stretched backbone chains. This is an important characteristic for piezoelectric properties. There are three other β peaks at $2\theta = 35.5°$, 40.8°, and 54.9°, indicating the (120), (220), and (221) planes, respectively. The intensity of the (200) peak increased with TPM, showing a maximum at 400 TPM. As the nanofibers were drawn, the polymer chains were accordingly stretched and aligned, showing greater proportions of β phase after spinning. The diffractogram also contains α peaks at $2\theta = 17.5°$ and 28.6° corresponding to the (020) and (001) planes, respectively. As with the (200) peak, the intensity of the (020) peak also increased with increasing TPM, indicating an overall enhancement in crystallinity.

DSC and FTIR analyses were used to quantify the crystallinity and β phase fraction of the nanofibers in each web and yarn. PVDF-TrFE exhibits a Curie transition and melts within a range of temperatures from 100 to 170 °C (Fig. 4b). Note that the Curie temperature refers to the temperature where ferroelectric domains break into paraelectric domains. The endothermic peaks at approximately 120 and 160 °C in the DSC thermogram of web nanofibers indicate the Curie temperature and the melting temperature, respectively. The Curie temperature, initially 122.5 °C, decreased to 106.5–110.8 °C after the nanofibers had been pulled and twisted into piezoelectric yarns. Lower Curie temperatures indicate smaller ferroelectric domains [43–45]. However, although both the Curie and melting temperatures of our nanofibers decreased after being spun into yarns, the intensity of their melting peaks increased. The area of the melting peak can be used to calculate the degree of crystallinity using the following relationship,

$$X_c = \frac{\Delta H_f}{\Delta H_f^*} \times 100 \tag{2}$$

where X_c is the percent crystallinity of the piezoelectric nanofiber or yarn, ΔH_f is the fusion enthalpy of a PVDF-TrFE yarn (Fig. S6), and ΔH_f^* is the fusion enthalpy of pure crystalline PVDF-TrFE. Here, the fusion enthalpy of the pure crystal was assumed to be equal to that of pure PVDF (104.7 J/g) [46,47]. The crystallinity of PVDF-TrFE nanofibers in the web was 49.1%, while those of nanofibers in the yarns increased by 27%, 43%, 66%, and 83% for yarns formed at 1000, 800, 600, and 400 TPM, respectively. Interestingly, the crystallinity of 200 TMP yarns decreased by 93%, which is lower than that of nanofibers in the web. High translational speeds (5 mm/s) during spinning may have resulted in decreased crystallinity because excessive strain rates can break the crystal structure of nanofibers in the yarn. Crystallinity increased with yarn spinning with translational speeds up to 2.5 mm/s (400 TPM case). Despite its broader melting peak, which indicates a broader distribution of crystalline domain size, the increase rate of crystallinity of 400 TPM yarn (83%) was greater than that of 600 TPM yarn (66%). The lower melting temperature was attributed to an α - β phase transition. The melting temperature of the α phase (169 °C) is slightly higher than that of the β phase (167 °C) because the α phase is entropically more stable [48]. Therefore, a decrease in melting temperature can indicate an increase in the β phase fraction. The crystallinity of PVDF-TrFE nanofiber yarn is higher than those of PVDF nanofiber yarns because TrFE component can enhance the crystallinity and β phase ratio due to the large fluorine (F) atoms. The repulsive force between F atoms in TrFE component induces the stretch of the backbone chain of PVDF-TrFE [49–51].

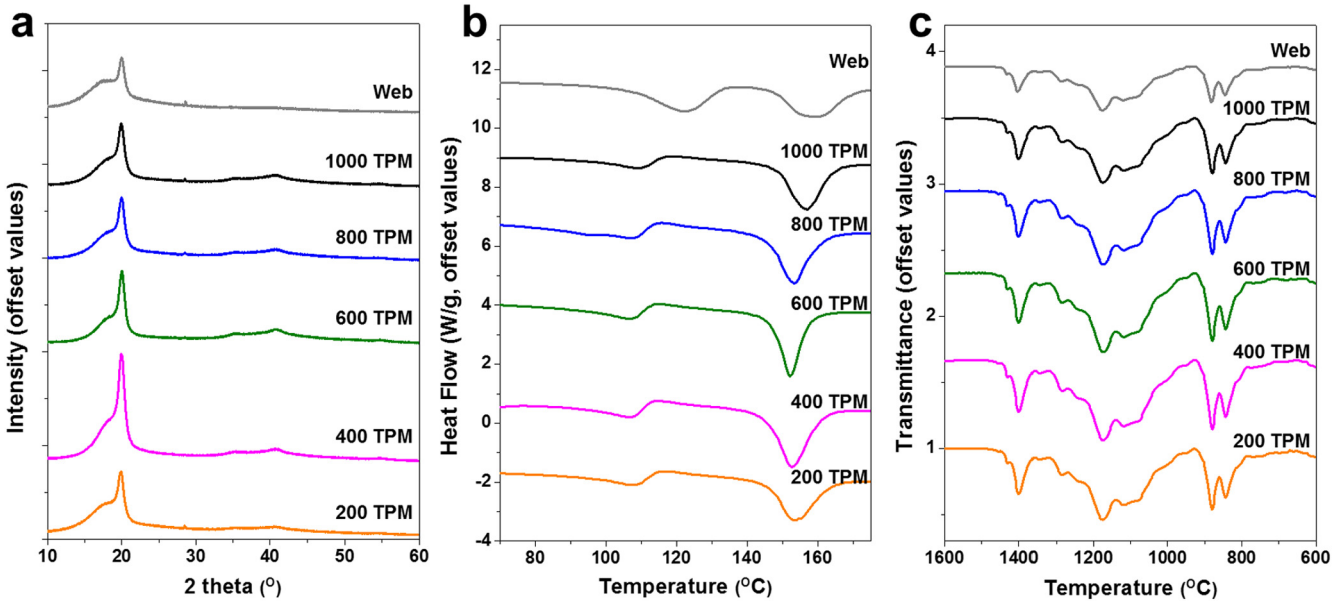

Fig. 4. Structural characterization of PVDF-TrFE nanofibers in the preform web and yarns: (a) X-ray diffraction (XRD), (b) differential scanning calorimetry (DSC), and (c) Fourier-transform infrared spectroscopy (FT-IR).

Therefore, PVDF-TrFE has been widely used in the piezoelectric fibers. The crystallinity of the PVDF-TrFE nanofibers in web was similar to the value of PVDF-TrFE nano/microfibers (~50%) in other studies [29,52], however it was enhanced by the stretching effect during yarn spinning process.

The phase fractions of PVDF-TrFE yarns were quantitatively evaluated by FTIR spectroscopy. The FTIR spectra in Fig. 4c contain six significant peaks, each corresponding to bond vibrations in either the α or β phase: 763α, 843β, 893β, 976α, 1280β, and 1404β. Since each peak corresponds to a single phase, their relative intensities can be used to quantify the mass fraction of each phase. Bands 763α and 843β were used to calculate the weight fraction of the β phase as follows [53–55].

$$F(\beta) = \frac{X_\beta}{X_\alpha + X_\beta} = \frac{A_\beta}{(K_\alpha/K_\beta)A_\alpha + A_\beta} = \frac{A_\beta}{1.26A_\alpha + A_\beta} \quad (3)$$

where F(β) is the β phase fraction in the material, *X* is the mass fraction, *A* is the absorption band intensity, and *K* is the absorption coefficient of each phase. F(β) of PVDF-TrFE nanofibers in the web was 0.775, increasing to 0.812, 0.832, 0.852, 0.871, and 0.827 for nanofibers in yarns spun at 1000, 800, 600, 400, and 200 TPM, respectively. Thus, the weight fraction of the β phase increased after yarn spinning. Since TrFE component can enhance F(β) [49–51], as-spun PVDF-TrFE nanofibers showed high β phase ratio (ca. 0.77), which is similar value to those of PVDF nanofibers (ca. 0.79) stretched after electrospinning [52]. In our study, the nanofibers in web showed a similar F(β) of 0.78 and the amount of β phase increased after the yarn spinning process. Note that the highest F(β) was observed in yarns spun at 400 TPM, which is consistent with the results of XRD, Curie temperature, and crystallinity analyses. As noted above in the DSC analysis, the melting temperature of PVDF-TrFE decreases with increased β phase content. The amount of β phase, which is closely related to piezoelectric behavior, was calculated by multiplying the crystallinity obtained from DSC measurements with the β phase fraction obtained from FTIR analyses (Table S1). Although the difference in β phase fraction between the different yarns is much smaller than the differences in crystallinity, 400 PM yarns contained the highest amount of β phase.

3.3. Mechanical properties

The mechanical robustness of piezoelectric yarns is an important parameter in the manufacture of piezoelectric textiles. Single-strand tensile tests (Fig. S1) were used to characterize the mechanical properties of our PVDF-TrFE yarns. The data in Fig. 5a show that the yarns exhibited elasto-plastic behaviors. With the exception of the 200 TPM yarn, strains were more than 100%. Elongation at break decreased with increasing translational speeds, i.e., low TPM conditions. Twist angles and yarn diameters decreased as the translational speed of the twisting motor increased. Therefore, yarns that had already been stretched by high translational speeds during spinning exhibited low elongation limits. In contrast, the ultimate tensile strength of the yarns was highest at 800 TPM (Table S2), with Young's modulus in the elastic region showing the same trend. The tensile strength (24.3 MPa) and Young's modulus (110.1 MPa) of PVDF-TrFE yarn were similar to those of PVDF nanofiber yarn made by electrospun ribbon (22.1 MPa and 115 MPa) [35].

In this study, 400 TPM yarn was expected to show the maximum in tensile properties because the modulus of β phase was higher than that of α phase in material properties [56]. However, our 400 TPM yarns exhibited very low modulus and strength. This can be explained in terms of yarn mechanics. The tensile strength of twisted yarns is known to follow Hearle's theory [57,58], which states that the tensile properties of a yarn, particularly those related to stress, such as strength and modulus, are optimal at a specific twist angle because of trade-offs between obliquity and inter-yarn frictional forces generated by the application of a lateral force. The tensile strength of nanofiber yarns has been shown to follow Hearle's theory regardless of diameter [59–62]. In yarn mechanics, the highest modulus and strength values are generally observed at a surface angle around 35°. In the current study, the maximum tensile strength and modulus were observed with yarns fabricated at 800 TMP (Fig. 5b), resulting in a surface angle of 37.9°. The surface angles of yarns generated at 1000, 600, 400, and 200 TPM were 46.9°, 30.2°, 22.8°, and 15.7°, respectively. These data confirm that the tensile strength and modulus of a piezoelectric yarn is governed by its twist structure and surface angle.

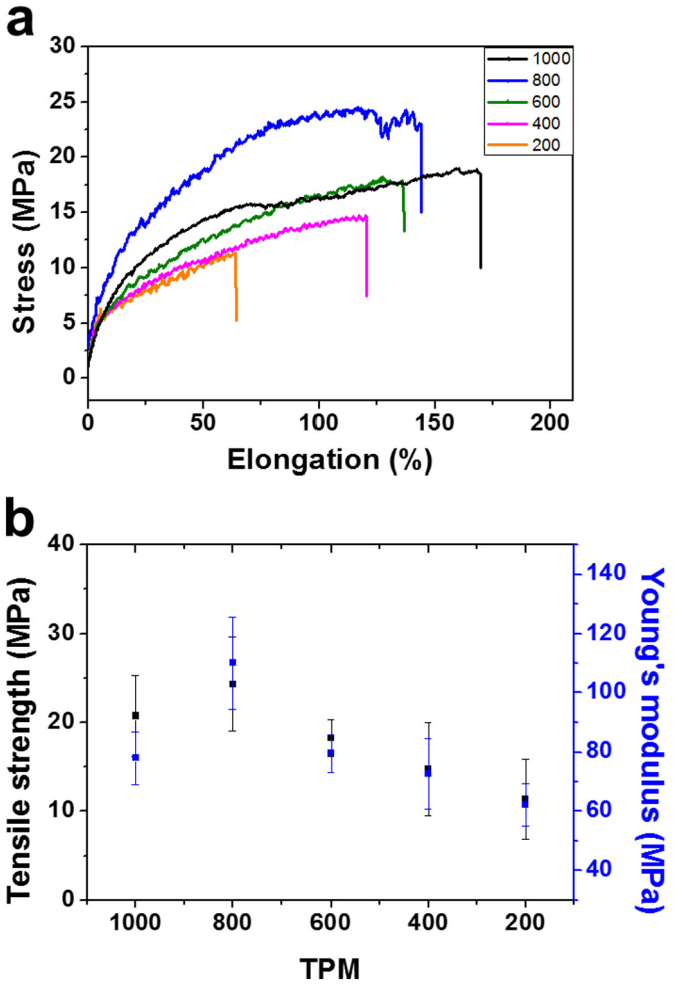

Fig. 5. (a) Tensile stress–strain curves and (b) tensile moduli and strengths are shown for piezoelectric yarns as functions of translational speed during the spinning process.

3.4. Piezoelectric properties

The polarization direction of PVDF is orthogonal to the backbone chain. The backbone chains of PVDF molecules in PVDF fibers created via electrospinning and subsequent yarn twisting run parallel to the primary axis of the fiber. Therefore, to assess the piezoelectric properties of these yarns, a compressive stress was applied transverse to the fiber axis. Three layers of piezoelectric yarns were prepared and tested, yielding piezoelectric potentials of 500–600 mV under 1 MPa at 0.5 Hz. The piezoelectric potential was stable (constant) over 8 compression cycles (Fig. 6a). Note that the piezoelectric potentials of the yarns were lower than their corresponding thin films [63] due to the porous structure of yarn, which ensures flexibility and stretchability. In addition, 600 mV is high enough to for sensor or nanogenerator applications such as breath sensors and cochlear implants [16,19,20]. It is also worth mentioning that our piezoelectric yarns, which were manufactured without any additional polarization processes, generated greater potentials than

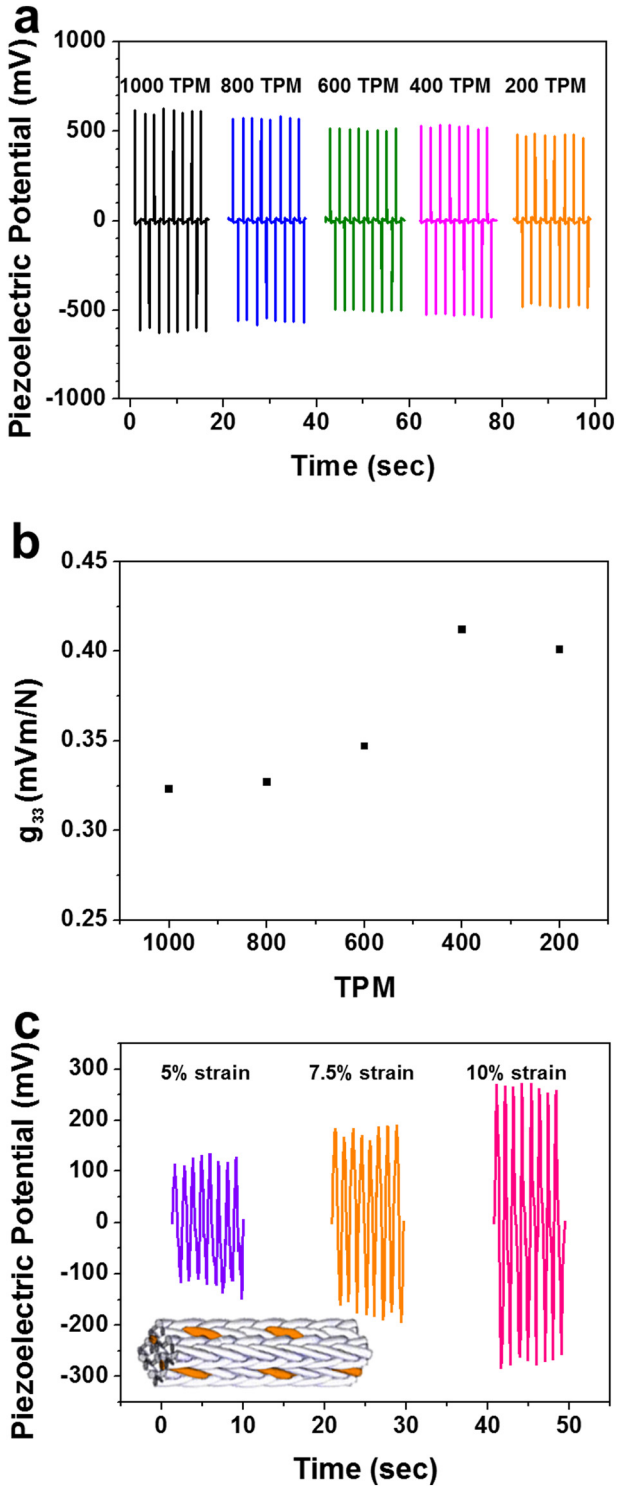

Fig. 6. (a) piezoelectric potentials and (b) piezoelectric voltage constants of PVDF-TrFE yarns are shown for a compressive stress of 1 MPa at 0.5 Hz. The PVDF-TrFE yarns were braided into 4 × 4 braid, and (c) the piezoelectric characterization of 3D piezoelectric braid was performed under 5–10% strain.

PVDF-TrFE yarns manufactured via melt spinning with poling (25 mV) [23], electrospinning with poling (520 mV) [29], and those formed into twisted nanofiber ribbons (20 mV) [30].

Despite having the lowest observed crystallinity and β phase fraction, the highest piezoelectric potential was observed with the 1000-TPM yarn. This phenomenon results from a change in the overall dipole moment of the yarn. The generated potential is proportional to the length of the dipole. Accordingly, the 1000-TPM yarn, which featured the largest diameter, exhibited the highest piezoelectric potential. To avoid any confusion from this extrinsic property, piezoelectric potentials should be normalized by the diameter of the yarn. Piezoelectric voltage constants (g_{33}) were therefore calculated using the following equation (and increasing mode in Fig. S7).

$$V(Q = 0) = g_{33}\, d\, \sigma \tag{4}$$

where V is the piezoelectric potential, Q is the piezoelectric charge, d is the diameter of a nanofiber yarn, and σ is the compressive stress applied at 0.5 Hz. An increasing rectangular function of compressive stress was used to measure the piezoelectric voltage constant. The piezoelectric voltage constants of 1000, 800, 600, 400, and 200 TPM-yarns were 0.323, 0.329, 0.0347, 0.412, and 0.401 mVm/N, respectively. The piezoelectric voltage constant of 0.41 mVm/N in our study was higher than that of electrospun PVDF nanofiber (0.38 mVm/N) [52]. The highest constant was observed with the 400-TPM yarn, which also exhibited the largest increase in degree of crystallinity (by 83%) and the highest proportion of β phase (by 12%) (Fig. 4). In addition, the low Young's modulus of the 400-TPM yarn proved advantageous, allowing for greater material deformation and higher piezoelectric voltages. Together, the high proportion of β phase crystals and large deformability resulted in enhanced intrinsic piezoelectric properties.

As an example of the piezoelectric yarns for piezoelectric textile, a 3D braid was manufactured using PVDF-TrFE nanofiber yarns with 400 TPM (~400 μm) and two copper wires (410 μm) as piezoelectric yarns and electrode wires, respectively, and a 4-step braid device built in lab (see Fig. S8 and S9). Yarns were provided at each carrier, which moved along the axial direction (Fig. S8c) every four steps (Fig. S8d). In the machine, 24 carriers with 22 PVDF-TrFE yarns and 2 copper wires were used for 4 × 4 piezoelectric braid. PVDF-TrFE yarns contacted with copper wires as electrodes, and the structure was very compact. The trace diagram and position of electrode wires in every 4 steps were shown in Fig. S9 (in the revised manuscript). The direction of compression between electrodes (i.e., direction of piezoelectric reaction) changed. Therefore, only poling-free piezoelectric yarns can be used for 3D braid. The piezoelectric performance of this braid was characterized by the tensile test of 5%, 7.5%, and 10% strain at 0.5 Hz. The two ends of the piezoelectric braid were taped with an insulation tape and two electrode wires were pulled out separately to measure the piezoelectric potential. The electrodes were connected to Keithley 6517B to measure the electrical potential. The piezoelectric potential of the 3D braid was 120 mV, 180 mV, and 260 mV for 5%, 7.5%, and 10% strain condition, respectively (Fig. Fig. 6c). This was possible because the yarns in the 3D braid tend to be straight in the axial direction by tension, imposing the compression on the piezoelectric yarns between electrode yarns. Unlike the yarns, the piezoelectric braids showed a triangular shape of potentials because they were not rectified. The piezoelectric responses were stable during 8 cycles and were almost proportional to the tensile strain. As tensile strain increased (i.e., deformation increased on the axial direction), the compressive force of PVDF-TrFE yarns between two electrodes became large, increasing the piezoelectric response.

4. Conclusions

Twist-spun piezoelectric yarns were developed using PVDF-TrFE electrospun nanofibers and subsequent yarning (twist-spinning). Randomly-oriented electrospun nanofiber webs were pulled and twist-spun with careful control of rotational and translational speeds during twist-spinning, resulting in piezoelectric yarns without any further poling operation. The crystallinity and β phase ratio of the nanofibers in the piezoelectric yarns increased by 83% compared to nanofibers in the preform web. Enhanced crystallinity (by 83%) and β phase ratio (by 12%) were achieved by a high stretching ratio (400 TPM). However, further stretching, e.g., 200 TPM, led to

deterioration of the crystal structure, and the related physical and piezoelectric properties, of the nanofibers. The mechanical properties of the piezoelectric yarns showed a strong dependence on the surface angle of the yarn, indicating that structural features, rather than the microstructure of individual constituent nanofibers, can determine the mechanical properties of piezoelectric yarns. Optimum piezoelectric yarns demonstrated a piezoelectric potential and a piezoelectric voltage constant of 550 mV and 0.412, respectively, due to high crystallinity and β phase ratio combined with a low Young's modulus.

CRediT authorship contribution statement

Sarang Park: Conceptualization, Methodology, Validation, Formal analysis, Investigation, Writing - original draft. **Youbin Kwon:** Conceptualization, Validation, Visualization. **Minchang Sung:** Conceptualization, Validation. **Byoung-Sun Lee:** Validation. **Jihyun Bae:** Validation. **Woong-Ryeol Yu:** Conceptualization, Writing - review & editing, Supervision, Project administration.

Acknowledgement

This work was supported by a National Research Foundation of Korea (NRF) grant funded by the Ministry of Education (MOE) (NRF-2016R1D1A1B03935554) and by an NRF grant funded by the Ministry of Science, ICT and Future Planning (MSIP) (No. NRF-2015R1A5A1037627). This work was also supported by a National Research Foundation of Korea (NRF) grant funded by the Korean Government (NRF-2018M3A7B4089670). The Institute of Engineering Research at Seoul National University provided research facilities for this work.

Appendix A. Supplementary data

Supplementary data to this article can be found online at https://doi.org/10.1016/j.matdes.2019.107889.

References

[1] J. Edmison, M. Jones, Z. Nakad, T. Martin, Using piezoelectric materials for wearable electronic textiles, Sixth International Symposium on Wearable Computers (2002) 41–48.
[2] D. Yun, K.-S. Yun, Woven piezoelectric structure for stretchable energy harvester, Electron. Lett., Institution Eng. Technol. (2013) 65–66.
[3] K. Magniez, A. Krajewski, M. Neuenhofer, R. Helmer, Effect of drawing on the molecular orientation and polymorphism of melt-spun polyvinylidene fluoride fibers: toward the development of piezoelectric force sensors, J. Appl. Polym. Sci. 129 (5) (2013) 2699–2706.
[4] S. Song, K.-S. Yun, Design and characterization of scalable woven piezoelectric energy harvester for wearable applications, Smart Mater. Struct. 24 (4) (2015), 045008.
[5] A. Lund, K. Rundqvist, E. Nilsson, L. Yu, B. Hagström, C. Müller, Energy harvesting textiles for a rainy day: woven piezoelectrics based on melt-spun PVDF microfibres with a conducting core, npj Flex. Electron. 2 (1) (2018) 9.
[6] P. Hofmann, A. Walch, A. Dinkelmann, S.K. Selvarayan, G.T. Gresser, Woven piezoelectric sensors as part of the textile reinforcement of fiber reinforced plastics, Compos. A: Appl. Sci. Manuf. 116 (2019) 79–86.
[7] A. Atalay, O. Atalay, M.D. Husain, A. Fernando, P. Potluri, Piezofilm yarn sensor-integrated knitted fabric for healthcare applications, J. Ind. Text. 47 (4) (2017) 505–521.
[8] D. Matsouka, S. Vassiliadis, D.V. Bayramol, Piezoelectric textile fibres for wearable energy harvesting systems, Mater. Res. Express 5 (6) (2018), 065508.
[9] F. Mokhtari, J. Foroughi, T. Zheng, Z.X. Cheng, G.M. Spinks, Triaxial braided piezo fibers energy harvesters for self-powered wearable technologies, J. Mater. Chem. A 7 (2019) 8245–8257.
[10] B. Yang, K. Yun, Efficient energy harvesting from human motion using wearable piezoelectric shell structures, 2011 16th International Solid-State Sensors, Actuators and Microsystems Conference (2011) 2646–2649.
[11] Y. Tajitsu, Smart piezoelectric fabric and its application to control of humanoid robot, Ferroelectrics 499 (1) (2016) 36–46.
[12] B. Yang, K.-S. Yun, Piezoelectric shell structures as wearable energy harvesters for effective power generation at low-frequency movement, Sensors Actuators A Phys. 188 (2012) 427–433.
[13] M. Zhang, T. Gao, J. Wang, J. Liao, Y. Qiu, Q. Yang, H. Xue, Z. Shi, Y. Zhao, Z. Xiong, L. Chen, A hybrid fibers based wearable fabric piezoelectric nanogenerator for energy harvesting application, Nano Energy 13 (2015) 298–305.
[14] M. Lee, C.-Y. Chen, S. Wang, S.N. Cha, Y.J. Park, J.M. Kim, L.-J. Chou, Z.L. Wang, A hybrid piezoelectric structure for wearable Nanogenerators, Adv. Mater. 24 (13) (2012) 1759–1764.
[15] H. He, Y. Fu, W. Zang, Q. Wang, L. Xing, Y. Zhang, X. Xue, A flexible self-powered T-ZnO/PVDF/fabric electronic-skin with multi-functions of tactile-perception, atmosphere-detection and self-clean, Nano Energy 31 (2017) 37–48.
[16] N.P. Maria Joseph Raj, N.R. Alluri, V. Vivekananthan, A. Chandrasekhar, G. Khandelwal, S.-J. Kim, Sustainable yarn type-piezoelectric energy harvester as an eco-friendly, cost-effective battery-free breath sensor, Appl. Energy 228 (2018) 1767–1776.
[17] N. Weber, Y.S. Lee, S. Shanmugasundaram, M. Jaffe, T.L. Arinzeh, Characterization and in vitro cytocompatibility of piezoelectric electrospun scaffolds, Acta Biomater. 6 (9) (2010) 3550–3556.
[18] L.T. Beringer, X. Xu, W. Shih, W.-H. Shih, R. Habas, C.L. Schauer, An electrospun PVDF-TrFe fiber sensor platform for biological applications, Sensors Actuators A Phys. 222 (2015) 293–300.
[19] C. Mota, M. Labardi, L. Trombi, L. Astolfi, M. D'Acunto, D. Puppi, G. Gallone, F. Chiellini, S. Berrettini, L. Bruschini, S. Danti, Design, fabrication and characterization of composite piezoelectric ultrafine fibers for cochlear stimulation, Mater. Des. 122 (2017) 206–219.
[20] N. Mukherjee, R.D. Roseman, J.P. Willging, The piezoelectric cochlear implant: concept, feasibility, challenges, and issues, J. Biomed. Mater. Res. 53 (2) (2000) 181–187.
[21] K.R. Brain, Investigations of piezo-electric effects with dielectrics, Proc. Phys. Soc. Lond. 36 (1) (1923) 81–93.
[22] H. Kawai, The piezoelectricity of poly (vinylidene fluoride), Jpn. J. Appl. Phys. 8 (7) (1969) 975–976.
[23] D. Matsouka, S. Vassiliadis, K. Prekas, D.V. Bayramol, N. Soin, E. Siores, On the measurement of the electrical power produced by melt spun piezoelectric textile Fibres, J. Electron. Mater. 45 (10) (2016) 5112–5126.
[24] D. Matsouka, S. Vassiliadis, D. Vatansever Bayramol, N. Soin, E. Siores, Investigation of the durability and stability of piezoelectric textile fibres, J. Intell. Mater. Syst. Struct. 28 (5) (2017) 663–670.
[25] J. Ning, M. Yang, H. Yang, Z. Xu, Tailoring the morphologies of PVDF nanofibers by interfacial diffusion during coaxial electrospinning, Mater. Des. 109 (2016) 264–269.
[26] Z. Li, Y. Xu, L. Fan, W. Kang, B. Cheng, Fabrication of polyvinylidene fluoride tree-like nanofiber via one-step electrospinning, Mater. Des. 92 (2016) 95–101.
[27] L. Serairi, L. Gu, Y. Qin, Y. Lu, P. Basset, Y. Leprince-Wang, Flexible piezoelectric nanogenerators based on PVDF-TrFE nanofibers, Eur. Phys. J. Appl. Phys. 80 (3) (2017), 30901.
[28] L. Persano, C. Dagdeviren, Y. Su, Y. Zhang, S. Girardo, D. Pisignano, Y. Huang, J.A. Rogers, High performance piezoelectric devices based on aligned arrays of nanofibers of poly(vinylidenefluoride-co-trifluoroethylene), Nat. Commun. 4 (2013) 1633.
[29] H. Gao, P.T. Minh, H. Wang, S. Minko, J. Locklin, T. Nguyen, S. Sharma, High-performance flexible yarn for wearable piezoelectric nanogenerators, Smart Mater. Struct. 27 (9) (2018), 095018.
[30] M. Baniasadi, J. Huang, Z. Xu, S. Moreno, X. Yang, J. Chang, M.A. Quevedo-Lopez, M. Naraghi, M. Minary-Jolandan, High-performance coils and yarns of polymeric piezoelectric nanofibers, ACS Appl. Mater. Interfaces 7 (9) (2015) 5358–5366.
[31] E. Yang, Z. Xu, L.K. Chur, A. Behroozfar, M. Baniasadi, S. Moreno, J. Huang, J. Gilligan, M. Minary-Jolandan, Nanofibrous smart fabrics from twisted yarns of electrospun piezopolymer, ACS Appl. Mater. Interfaces 9 (28) (2017) 24220–24229.
[32] D. Mandal, S. Yoon, K.J. Kim, Origin of piezoelectricity in an electrospun poly (vinylidene fluoride-trifluoroethylene) nanofiber web-based nanogenerator and nano-pressure sensor, Macromol. Rapid Commun. 32 (11) (2011) 831–837.
[33] D. Mandal, K. Henkel, D. Schmeißer, Improved performance of a polymer nanogenerator based on silver nanoparticles doped electrospun P (VDF–HFP) nanofibers, Phys. Chem. Chem. Phys. 16 (22) (2014) 10403–10407.
[34] S.-H. Park, H.B. Lee, S.M. Yeon, J. Park, N.K. Lee, Flexible and stretchable piezoelectric sensor with thickness-tunable configuration of electrospun nanofiber mat and elastomeric substrates, ACS Appl. Mater. Interfaces 8 (37) (2016) 24773–24781.
[35] R. Nakashima, K. Watanabe, Y. Lee, B.-S. Kim, I.-S. Kim, Mechanical properties of poly (vinylidene fluoride) nanofiber filaments prepared by electrospinning and twisting, Adv. Polym. Technol. 32 (S1) (2013) E44–E52.
[36] M. Yousefzadeh, M. Latifi, W.E. Teo, M. Amani-Tehran, S. Ramakrishna, Producing continuous twisted yarn from well-aligned nanofibers by water vortex, Polym. Eng. Sci. 51 (2) (2011) 323–329.
[37] T. Yan, L. Tian, Z. Pan, Structures and mechanical properties of plied and twisted polyacrylonitrile nanofiber yarns fabricated by a multi-needle electrospinning device, Fibers Polym. 17 (10) (2016) 1627–1633.
[38] L. Tian, T. Yan, Z. Pan, Fabrication of continuous electrospun nanofiber yarns with direct 3D processability by plying and twisting, J. Mater. Sci. 50 (21) (2015) 7137–7148.
[39] U. Ali, Y. Zhou, X. Wang, T. Lin, Direct electrospinning of highly twisted, continuous nanofiber yarns, J. Text. Inst. 103 (1) (2012) 80–88.
[40] E. Ahmadloo, A. Gharehaghaji, M. Latifi, N. Mohammadi, H. Saghafi, How fracture toughness of epoxy-based nanocomposite is affected by PA66 electrospun nanofiber yarn, Eng. Fract. Mech. 182 (2017) 62–73.
[41] E. Ahmadloo, A. Gharehaghaji, M. Latifi, H. Saghafi, N. Mohammadi, Effect of PA66 nanofiber yarn on tensile fracture toughness of reinforced epoxy nanocomposite, Proc. Inst. Mech. Eng. C J. Mech. Eng. Sci. 233 (6) (2019) 2033–2043.

[42] M.N. Shuakat, T. Lin, Direct electrospinning of nanofibre yarns using a rotating ring collector, J. Text. Inst. 107 (6) (2016) 791–799.
[43] R.A. Whiter, Y. Calahorra, C. Ou, S. Kar-Narayan, Observation of confinement-induced self-poling effects in ferroelectric polymer nanowires grown by template wetting, Macromol. Mater. Eng. 301 (9) (2016) 1016–1025.
[44] Y. Zhang, S. Tan, J. Wang, X. Wang, W. Zhu, Z. Zhang, Regulating dielectric and ferroelectric properties of poly(vinylidene fluoride-trifluoroethylene) with inner CH= CH bonds, Polymers 10 (3) (2018) 339.
[45] Y. Chen, L. Zhang, J. Liu, X. Lin, W. Xu, Y. Yue, Q.-D. Shen, Ferroelectric domain dynamics and stability in graphene oxide-P(VDF-TrFE) multilayer films for ultra-high-density memory application, Carbon 144 (2019) 15–23.
[46] F.O. Agyemang, F.A. Sheikh, R. Appiah-Ntiamoah, J. Chandradass, H. Kim, Synthesis and characterization of poly (vinylidene fluoride)–calcium phosphate composite for potential tissue engineering applications, Ceram. Int. 41 (5) (2015) 7066–7072 Part B.
[47] M. Sharma, J.K. Quamara, A. Gaur, Behaviour of multiphase PVDF in (1− x) PVDF/ (x) BaTiO 3 nanocomposite films: structural, optical, dielectric and ferroelectric properties, J. Mater. Sci. Mater. Electron. 29 (2018) 10875–10884.
[48] R. Gregorio, N.C.P.d.S. Nociti, Effect of PMMA addition on the solution crystallization of the alpha and beta phases of poly(vinylidene fluoride) (PVDF), J. Phys. D. Appl. Phys. 28 (2) (1995) 432–436.
[49] Z. Cui, N.T. Hassankiadeh, Y. Zhuang, E. Drioli, Y.M. Lee, Crystalline polymorphism in poly (vinylidenefluoride) membranes, Prog. Polym. Sci. 51 (2015) 94–126.
[50] W. Doll, J. Lando, The polymorphism of poly (vinylidene fluoride) V. the effect of hydrostatic pressure on the melting behavior of copolymers of vinylidene fluoride, J. Macromol. Sci., Part B: Phys. 4 (4) (1970) 897–913.
[51] N. Hernandez, V. González-González, I. Dzul-Bautista, N. Ornelas-Soto, J. Barandiarán, J. Gutierrez, Electrospun poly (vinylidene fluoride-trifluoroethylene) based flexible magnetoelectric nanofibers, Eur. Polym. J. 109 (2018) 336–340.
[52] M. Abbasipour, R. Khajavi, A.A. Yousefi, M.E. Yazdanshenas, F. Razaghian, The piezoelectric response of electrospun PVDF nanofibers with graphene oxide, graphene, and halloysite nanofillers: a comparative study, J. Mater. Sci. Mater. Electron. 28 (21) (2017) 15942–15952.
[53] M. Wu, H.-X. Huang, J. Tong, Enhancing β-phase content and tensile properties in poly(vinylidene fluoride) by adding halloysite nanotubes and injecting water during extrusion, Mater. Des. 108 (2016) 761–768.
[54] N. Abzan, M. Kharaziha, S. Labbaf, Development of three-dimensional piezoelectric polyvinylidene fluoride-graphene oxide scaffold by non-solvent induced phase separation method for nerve tissue engineering, Mater. Des. 167 (2019), 107636.
[55] H. Parangusan, D. Ponnamma, M.A.A. Al-Maadeed, Stretchable electrospun PVDF-HFP/co-ZnO nanofibers as piezoelectric Nanogenerators, Sci. Rep. 8 (1) (2018) 754.
[56] G. Suresh, S. Jatav, G. Mallikarjunachari, M.S.R. Rao, P. Ghosh, D.K. Satapathy, Influence of microstructure on the nanomechanical properties of polymorphic phases of poly(vinylidene fluoride), J. Phys. Chem. B 122 (36) (2018) 8591–8600.
[57] J.W. Hearle, P. Grosberg, S. Backer, Structural Mechanics of Fibers, Yarns, and Fabrics, 1969.
[58] J.W. Hearle, B. Lomas, W.D. Cooke, Atlas of Fibre Fracture and Damage to Textiles, Elsevier, 1998.
[59] H. Yan, L. Liu, Z. Zhang, Continually fabricating staple yarns with aligned electrospun polyacrylonitrile nanofibers, Mater. Lett. 65 (15) (2011) 2419–2421.
[60] Z. Xie, H. Niu, T. Lin, Continuous polyacrylonitrile nanofiber yarns: preparation and dry-drawing treatment for carbon nanofiber production, RSC Adv. 5 (20) (2015) 15147–15153.
[61] S.J. Najafi, A.A. Gharehaghaji, S.M. Etrati, Fabrication and characterization of elastic hollow nanofibrous PU yarn, Mater. Des. 99 (2016) 328–334.
[62] H. Maleki, A.A. Gharehaghaji, P.J. Dijkstra, Electrospinning of continuous poly (L-lactide) yarns: effect of twist on the morphology, thermal properties and mechanical behavior, J. Mech. Behav. Biomed. Mater. 71 (2017) 231–237.
[63] V. Bhavanasi, V. Kumar, K. Parida, J. Wang, P.S. Lee, Enhanced piezoelectric energy harvesting performance of flexible PVDF-TrFE bilayer films with graphene oxide, ACS Appl. Mater. Interfaces 8 (1) (2015) 521–529.